

# Multiscale Simulations of Carbon Nanotube Nucleation and Growth: Mesoscopic Continuum Calculations

S. Pannala<sup>a</sup> and R. F. Wood<sup>b, \*</sup>

<sup>a</sup>Computer Science and Mathematics Division, Oak Ridge National Laboratory, Oak Ridge, Tennessee, USA

<sup>b</sup>Condensed Matter Sciences Division, Oak Ridge National Laboratory, Oak Ridge, Tennessee, USA

As part of a focused computational effort on the multiscale simulations of carbon nanotube nucleation and growth, we have developed computer programs for coupled heat and mass flow in one and two dimensions. In the tip-growth mode, the sample is divided into three main regions, each of which can be further subdivided as required. In region 1, carbon is supplied to the catalytic particle from an ambient gas of carbon-containing compounds. The chemistry and thermodynamics of the decomposition of these compounds can be included in region 1, but the capability has not yet been implemented. The carbon diffuses through the catalytic particle in region 2 under concentration and temperature gradients and with a diffusion coefficient that can depend on both concentration and temperature. Region 3 consists of the interfacial region between the catalytic particle and the growing nanotube. Results to date demonstrate the key roles played by the size and shape of the catalytic particle in conjunction with the concentration and temperature gradients at the gas/solid interface and in region 2. Results also suggest how the growth of a single wall may interfere with, but not necessarily prevent, the growth of additional walls in a multi-walled nanotube. Again, the carbon concentration profile in the catalytic particle at the different growth sites is a key factor.

**Keywords:** Carbon Nanotubes, Growth Modeling, Continuum Modeling, Multiscale Modeling, Tip Growth, Root Growth, Carbon Diffusion into Nickel.

## 1. INTRODUCTION

It is difficult to exaggerate the potential importance of carbon nanoscience and particularly carbon nanotubes (CNTs) and nanofibers to the future of advanced materials development.<sup>1, 2</sup> Nanotubes are lightweight and exceptionally strong and have excellent thermal properties. Their incorporation into composite materials could revolutionize a wide range of advanced structural materials. Likewise their electronic properties, particularly of single-walled carbon nanotubes (SWNTs), have proved to be fascinating by exhibiting electrical conductivity that varies from metallic to semiconducting to insulating, depending on the growth conditions. It has also been claimed that CNTs are excellent as a storage medium for atomic hydrogen. Although this claim is now considered rather controversial, its implications for a hydrogen-based energy economy could be profound. Unfortunately, there are intimidating roadblocks in the path to the development and commercialization of technologies based on CNTs. As yet, there are no established methods for growing nanotubes in the quantities and with the purity needed. And once grown, the separation of

various types (single-walled, multi-walled, aligned, etc.) is time-consuming, unreliable, and costly. Also, there is no way at this time to control the electrical properties by growing nanotubes with specified diameter, length, and chirality. The recent notion<sup>3-5</sup> is that bulk quantities of quality SWNTs and multi-walled nanotubes (MWNTs) can be obtained by use of chemical vapor deposition (CVD), and we limit the current study to this process. Once the model is established, it can be extended to other production processes.

It is widely agreed that a much better understanding of the nucleation and growth processes is needed. Because *in situ* techniques for directly observing the growth are not mature, "multi-scale modeling and simulation" of the processes at some level is almost mandatory. In fact, research into simulations of such complex processes using high-performance computing is presently at the forefront of condensed matter science. Unfortunately, the time and space scales cover many orders of magnitude and the mathematical and computational aspects of such problems are formidable. For example, first-principles, quantum mechanical molecular dynamics (MD) calculations extensive enough for reliable parametric studies, even on a picosecond time scale, are well beyond the capabilities of current computers. Conversely, classical interaction potentials for dissimilar atoms

\*Author to whom correspondence should be addressed.

embedded in a complex atomic environment, which might greatly speed up the MD calculations, have proved virtually impossible to construct. Consequently, the multi-scaling used thus far for the type of problems addressed here is at a relatively modest level.

In the work described in this article attention has been focused on a mesoscopic continuum model, with inputs taken from experiment. However, in a companion paper presented at this workshop, first-principles atomistic calculations were used to obtain quantities that could become input data in future simulations. Well down the road one could imagine “seamlessly” transitioning between the various time and length scales. Whatever the approach, one of the first goals of any simulation should be to determine precisely the role of the catalytic particle and how it nucleates and controls the subsequent growth. To this end, we describe very briefly in the next section a continuum model introduced several years ago that seems to address most of the essential elements of the growth process (although not the nucleation step itself). Even though the model itself is quite simple, it is powerful in giving good insight into the diffusion of the carbon through the catalyst particle and understanding the rate-limiting steps. In Section III, the mathematical formulation of the model that we used is described and in Section IV extensive results of the type that are expected to be of interest to experimentalists are given. The article concludes with a summary and brief plan for future work.

## 2. BACKGROUND

We show in Figure 1 the model proposed by Baker and others for the so-called tip-growth mode.<sup>6–10</sup> The catalytic particle of some transition metal elements or alloys (e.g., Ni, Co, and Fe) frequently is represented as a truncated cone, out of which the nanotube grows. Carbon must be supplied at the top surface from some carbon-containing gas that is “cracked” at the surface. It is convenient to think of the schematic diagram of Figure 1 as being divided into three regions. Region 1, which is not explicitly shown on the figure and is not used in the calculations of this paper, will eventually incorporate a description of the gas-phase reactions just above the catalytic particle. It may also allow for the formation of solid-phase carbon compounds just at the interface with the catalytic particle. Region 2 contains the catalytic particle itself and is the focus of the present work, whereas region 3 contains the interfacial region between the catalyst and the growing CNT. It is not necessary to have a separate region for the nanotube itself, which is assumed to be completely formed as it emerges from region 3.

Then, with reference to Figure 1, a number of questions immediately come to mind. What are the decomposition rates of the carbon-containing gas in region 1 and how do they depend on the composition of the gas? How do the rates depend on temperature? Does formation of carbides

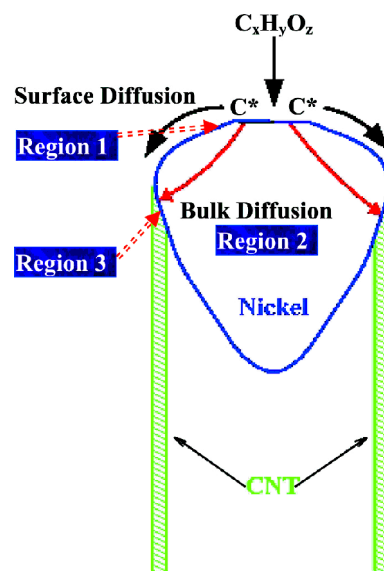


**Fig. 1.** Tip-growth mechanism. This was originally proposed by Baker for carbon nanofibers and now is a reasonably accepted mechanism for CNTs.

on the surface play a role and how stable are the carbides? What are the diffusion pathways, that is, surface or bulk? Is the growth rate diffusion limited, even for small catalytic particles? Is there something that might be called catalyst clogging? Does the carbon diffusion coefficient depend strongly on the concentration of carbon in the catalyst? Are there barriers and therefore activation energies for the precipitation of carbon into the CNT? How does precipitation start? Could it be a rate-limiting step? What dictates the chirality, diameter, and length? We hope to begin to answer some of these questions here and in the continuation of the research to be described in subsequent reports.

We note that the integration of first-principles atomistic calculations with the mesoscopic continuum calculations is expected to occur in several areas. First, the question of how the diffusion coefficient in region 2 depends on the carbon concentration is an important issue, especially for nanoparticles. This dependence is not easily measured experimentally, and it is not readily calculated because reliable classical interaction potentials are not available (see the article by Wells et al. in this issue). Secondly, all interfacial transition rates between the various regions should be obtained from electronic structure calculations of the activation energies. Finally, any dependence of the carbon ring formation on the presence of carbon atoms in the neighboring lattices has to be quantified and included to fully capture the nanotube formation and growth.

## 3. MESOSCOPIC CONTINUUM MODEL

Previous continuum modeling efforts<sup>11–13</sup> were focused on the growth of carbon filaments and fibers rather than single and MWNTs. In carbon filament growth, the carbon diffu-

sion through the rather large catalytic particle is usually the rate-limiting step, and thus those studies cannot be extrapolated simply to the CNT growth.<sup>14</sup> Also, using the latest advances in computational methods such as the finite element method with unstructured grids and adaptive mesh refinement (AMR), one can now simulate more complicated shapes and sizes of catalyst particles very efficiently. In the studies described here, the partial differential equation toolbox of MATLAB from Mathworks has been used to prototype the diffusion calculations in region 2 on two-dimensional (2D) unstructured grids. In the 2D unstructured grids used in the current simulation, any given shape is filled with triangular elements leading to a boundary conforming grid. The quality of the triangular elements can be controlled to ensure good numerical solution. Later, the complexity of the calculations can readily be extended to include interfacial dynamics arising from incorporating regions 1 and 3 in Figure 1. Region 1 can be modeled by simple rate equations with barriers. Region 3 requires detailed experimental and first-principles calculations to understand and model the incorporation of carbon atoms into the nanotube. As the model becomes more complicated, more inputs will be needed from experiments and first-principles calculations. At the current time enough information is not available to form a simple model for regions 1 and 3 and thus we restrict ourselves to region 2.

The diffusion equations for carbon concentration in terms of its mass fraction and the temperature can be written in cylindrical coordinates in the following forms:

$$\frac{\partial Y_c}{\partial t} + \frac{1}{r} \frac{\partial}{\partial r} \left( rD(T, Y_c) \frac{\partial Y_c}{\partial r} \right) + \frac{1}{r} \frac{\partial}{\partial z} \left( rD(T, Y_c) \frac{\partial Y_c}{\partial z} \right) = 0$$

$$\frac{\partial T}{\partial t} + \frac{1}{r} \frac{\partial}{\partial r} \left( rk(T) \frac{\partial T}{\partial r} \right) + \frac{1}{r} \frac{\partial}{\partial z} \left( rk(T) \frac{\partial T}{\partial z} \right) = 0$$
(1)

where  $Y_c$  is the carbon mass fraction,  $t$  is time,  $r$  is the radial coordinate,  $z$  is the axial coordinate,  $D$  is the diffusion coefficient,  $k$  is the thermal conductivity, and  $T$  is the temperature.

The diffusion coefficient is a function of both temperature and the carbon concentration. In the Ni–C system, experimental data are not available for the dependence of the diffusion coefficient on carbon concentration, and therefore for this study only the temperature dependence is considered. In the future, *ab initio* MD calculations that use density functional theory for computing the pertinent interaction parameters will be used to determine this dependence for a range of conditions applicable to the nanotube growth problem. The temperature dependence of the Ni–C system is of the following standard form for which the parameters can be found, for example, in the CRC materials handbook.<sup>15</sup>

$$D = D_0 e^{-\Delta E/kT}$$
(2)

The frequency factor ( $D_0$ ) for the present system is  $0.012 \text{ cm}^2 \text{ s}^{-1}$ , the activation energy,  $\Delta E$ , is  $34.0 \text{ kcal} \cdot \text{mol}^{-1}$  or  $1.46 \text{ eV/atom}$ , and  $k$  is the Boltzmann constant.

With the above simplification and with an assumption that the particle temperature field is uniform within the particle, Eq. 1 can be reduced to the following form:

$$\frac{\partial Y_c}{\partial t} + \frac{1}{r} \frac{\partial}{\partial r} \left( rD(T) \frac{\partial Y_c}{\partial r} \right) + \frac{1}{r} \frac{\partial}{\partial z} \left( rD(T) \frac{\partial Y_c}{\partial z} \right) = 0$$
(3)

Further, for steady-state calculations in which the time variation is not important, the above equation reduces to

$$\frac{\partial}{\partial r} \left( rD(T) \frac{\partial Y_c}{\partial r} \right) + \frac{\partial}{\partial z} \left( rD(T) \frac{\partial Y_c}{\partial z} \right) = 0$$
(4)

All of the results reported in this article were obtained using Eq. 4. Transient simulations were performed for a few cases, and the steady-state solution was typically reached within a few hundred milliseconds to at most a few seconds. The growth rates for CNTs are quite small ( $\sim \mu\text{m/s}$ ) and the time for growing several-millimeter-long CNTs is hundreds of seconds. For this reason, it is sufficient to use the steady-state solution for calculating growth rates.

The above equations are solved with appropriate boundary conditions (BCs). The schematic diagram with the BCs is shown in Figure 2. On the top surface ( $\text{C}_x\text{H}_y\text{O}_z$ -Ni interface), a Dirichlet BC in which the inlet carbon mass fraction is specified was assigned. This carbon mass fraction is not the carbon content of the CVD gases but the carbon fraction at the carbide layer/catalyst interface. The maximum solubility of carbon in Ni corresponds to  $\sim 5\%$  by mass, and we vary this between 0.5 to 5% to cover a realistic range. At the location where the nanotube is formed (NT–Ni interface), another Dirichlet BC is specified with

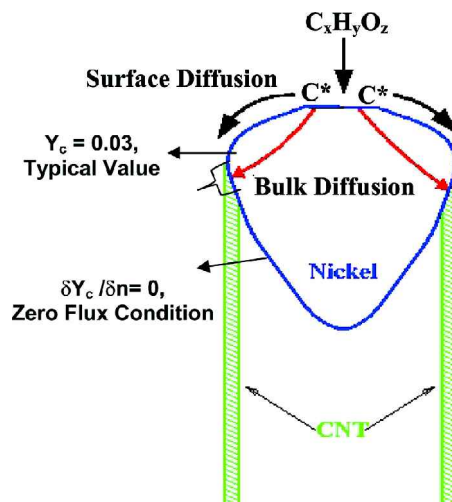


**Fig. 2.** Schematic diagram of the model problem with boundary conditions. The inlet surface and the location of CNT precipitation have Dirichlet BCs whereas the rest of the surfaces have zero-flux Neumann BCs.

**Table I.** Model inputs.

Diffusion rates
Temperature
Inlet composition
Shape of catalyst particle
Location of CNT formation
Size of catalyst

$Y_c$ , corresponding to a carbon activity of 1. From experimental correlations,<sup>12</sup> the carbon mass fraction corresponding to the carbon activity of 1 is determined and used in the simulations. This boundary condition is based on the earlier modeling work for the growth of carbon filaments.<sup>12, 13</sup> The typical value of the carbon mass fraction used for this BC is  $\sim 0.001$ . In the future, when more information is available about the catalyst–CNT interface, more accurate BCs can be prescribed with ease. We could have used flux conditions based on the known growth rates but that would have an implicit assumption that the process is diffusion control. The goal of this work is to determine the rate-limiting step rather than assuming one to start with. The outer radius of the nanotube corresponds to that of the Ni particle and an inner radius is determined by requiring the wall thickness to be 0.14 nm. On the rest of the Ni particle boundary, a Neumann BC with zero flux was specified.

The inputs to the model are listed in Table I. Once these inputs are specified, the above equations are solved until the specified convergence is reached. In the transient case, a solution is obtained and stored for each time step till the specified end time is reached. The typical output of the simulations is listed in Table II. The results from this model are described in the next section.

#### 4. RESULTS

A typical grid used in the simulations is shown in Figure 3. The 2D simulations are performed assuming symmetry across the centerline, as indicated in the figure. The geometry is constructed from one-half of the cross section of a truncated cone, with top and bottom surfaces closed in some specified manner with large radius curves. This geometry was chosen on the basis of a frequently observed shape of the catalyst.<sup>6, 16</sup> It was found that slight variations in the shape do not change the predictions drastically, and so this shape was fixed for all the simulations. Earlier 2D simulations<sup>12</sup> for carbon nanofibers used geometry quite similar to that of Figure 3, but with a simple, highly structured

**Table II.** Model predictions.

Spatio-temporal distribution of carbon
Inner diameter of NT
Single versus double versus multi-walled NTs
Growth rates
Insight into growth and control of NTs

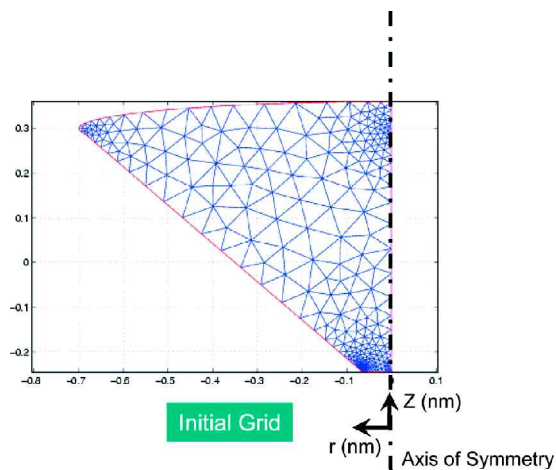


**Fig. 3.** Computational grid for a typical problem. The computations are performed using finite-element triangular elements. Only half of the domain is solved with centerline cylindrical symmetry. All the dimensions in this figure and other figures are in nanometers.

grid. Our grid takes advantage of the 2D space-filling characteristics of triangles that leads to very efficient numerical integration algorithms. This unstructured, adaptive grid is optimized simply by changing the size and shape of the triangular elements over the computational domain, as needed for convergence. In fact, for steady-state calculations, the AMR feature of the computer program can be used to refine the grid based on a variety of criteria. Here, we have chosen the criterion to be that the relative error of the solution at each point be smaller than a certain value. The final grid is similar to that of Figure 3, but with the triangle sizes and shapes adjusted accordingly. The computational time for steady-state calculations with around 10,000 elements typically is a few minutes on a Pentium IV 2.4 GHz desktop computer. The transient simulations take longer depending on the problem set-up.

The steady-state carbon concentration in the Ni particle for the SWNT growth is plotted in Figure 4. The carbon concentration at the top surface corresponds to the inlet boundary condition (as described by Figure 2 and explained earlier). The carbon concentration at the location of the growing nanotube corresponds to an activation coefficient of 1. In the transient simulation, as time proceeds, the carbon diffuses into the catalyst particle and the nanotube precipitates out when enough carbon is supplied to the interface where the tube is growing. The concentration in the rest of the particle almost reaches the inlet concentration. Thus, the entire particle acts like a reservoir for carbon, part of which diffuses into and is incorporated into the nanotube, whereas the deficit amount is replenished at the inlet source. This scenario, obtained from the steady-state solution and depicted in Figure 4, is also realized by running the transient simulation for extended times (seconds). The magnitude and direction of the corresponding carbon flux, superimposed on the contour map of concentration, are

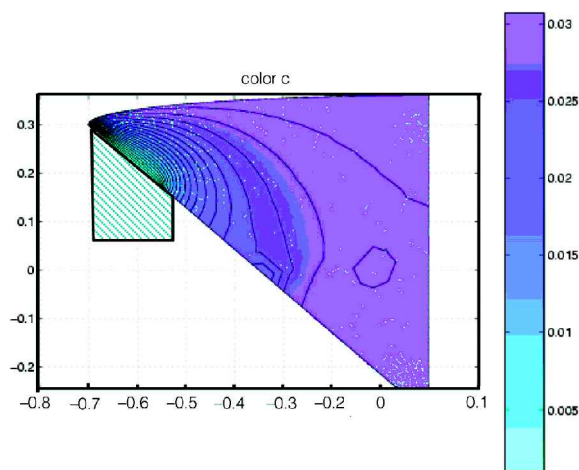


**Fig. 4.** Carbon concentration for the growth of SWNTs. The mass fraction legend is given on the right and ranges from 0 to 0.03. The location of the CNT is schematically shown on the figure. Corresponding mass fraction contours are shown for a clearer picture.

shown in Figure 5 by the array of arrows. It is clear that the largest gradients near the NT–Ni interface lead to maximum flux into the nanotube. These local gradients are important in determining the growth rates, rather than the average gradients calculated across the Ni particle.

Assuming axial symmetry, the gradient of the carbon concentration at the location of the CNT interface can be integrated to yield the effective growth rate for the tube. After such an exercise, one can estimate the growth rates of nanotubes under different conditions and so understand and identify the rate-limiting steps.

In the current simulations, three parameters are varied: inlet mass fraction, temperature of the catalyst particle, and the diameter of the Ni particle. In Figures 6–8, the variations

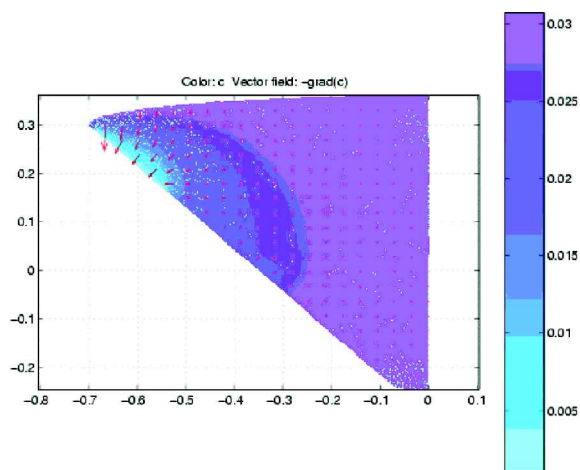


**Fig. 5.** Carbon concentration gradient for the growth of SWNTs. The arrows describe the direction of the gradient and the length of the arrows represents the magnitude. Carbon concentration is also superimposed on the figure to give a better representation.

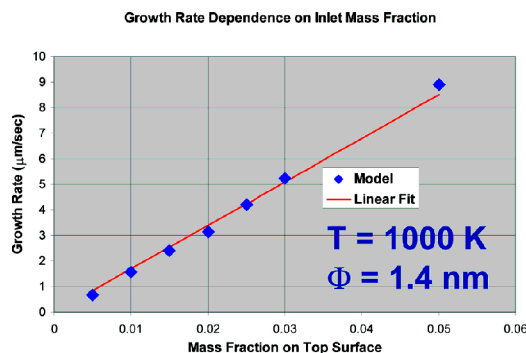


**Fig. 6.** Growth rate dependence on inlet carbon mass fraction for  $T = 1000\text{ K}$  and SWNT diameter = 10 nm. Here the inlet carbon mass fraction is varied, and the corresponding growth rate is plotted. There is linear dependence of growth rate with respect to inlet carbon mass fraction.

of growth rate were obtained by allowing one parameter to vary while the other two were fixed. Figure 6 shows the dependence of growth rate on the inlet concentration. The inlet source mass fraction determines the gradient of the carbon concentration as the carbon mass fraction at the precipitation location is fixed (based on carbon activity considerations), and this implies that any increase in the inlet carbon mass fraction will increase the gradient. Given this direct relationship, as expected, the growth of CNTs has linear dependence (a linear fit is drawn for comparison) on inlet carbon mass fraction as shown in Figure 6. This suggests that one way to increase the growth rates is to have surface conditions suitable to maintain higher carbon concentrations.

The dependence of growth rate on particle diameter is more complicated as shown in Figure 7. Here the growth rate decreases as the particle size increases. For large particles, the rate decreases drastically. From Figure 6, it is evident that the inlet carbon concentration drives the gradients that exist in the catalytic particle and thus controls the growth rate. The carbon diffused through the top surface of the catalyst particle depends on the surface area. From this surface, the carbon diffuses to fill in the entire volume of

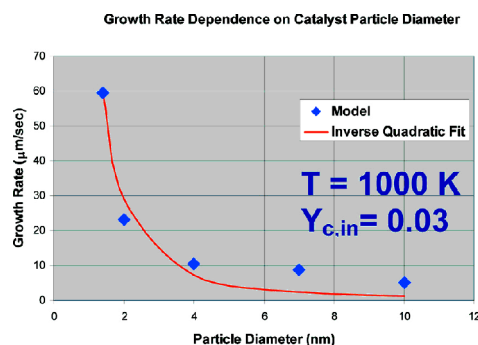


**Fig. 7.** Growth rate dependence on catalyst particle diameter for  $T = 1000\text{ K}$  and inlet carbon mass fraction = 0.03. Here the catalyst particle diameter is varied, and the corresponding growth rate is plotted. There is inverse quadratic dependence of growth rate with respect to particle diameter.

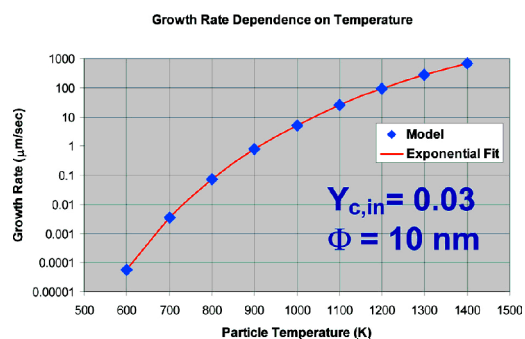


**Fig. 8.** Growth rate dependence on catalyst particle temperature for inlet carbon mass fraction = 0.03 and SWNT diameter = 10 nm. Here the particle temperature is varied, and the corresponding growth rate is plotted. There is an exponential relationship between growth rate and particle temperature.

the particle. The surface area varies as the square of the particle diameter, whereas the volume varies as the cube of the diameter. Consequently, the carbon concentration in the catalyst particle is inversely proportional to particle diameter. In addition, for the same carbon concentration at the inlet surface, the gradient varies inversely as the particle diameter (an inverse quadratic fit is drawn for comparison in Fig. 7). This explains the inverse quadratic dependence of growth rate on particle diameter and also the fast growth rates of small diameter SWNTs observed in some experiments.

In Figure 8 the dependence of growth rate on particle temperature is plotted. The carbon diffusion in the catalyst particle has an exponential dependence (Eq. 2) on temperature, and thus the growth rate, which is directly proportional to diffusion, has the expected exponential behavior (an exponential fit is plotted for comparison) as shown in Figure 8. The calculated growth rates in these numerical simulations are more than 1 order of magnitude different from those reported in some experiments<sup>16</sup> where the growth rate ( $\sim 0.001$ – $0.01 \mu\text{m/s}$ ) was measured indirectly. In very recent experiments, Geohegan et al.<sup>17</sup> measured growth rates ( $\sim 0.01$ – $0.3 \mu\text{m/s}$ ) directly by optical interference techniques. Their results are in much better agreement with the ones we show here for the temperature range used in the experiments. However, the rates reported in this article are slightly higher, as expected, because these are for the SWNTs rather than for the MWNTs formed in the experiment. For example, at 1000 K, Geohegan et al. reported a growth rate of  $0.3 \mu\text{m/s}$  whereas the model predicts  $2 \mu\text{m/s}$  with a surface carbon mass fraction of 0.01. Future studies will include the comparison of MWNT growth rates against this experimental dataset.

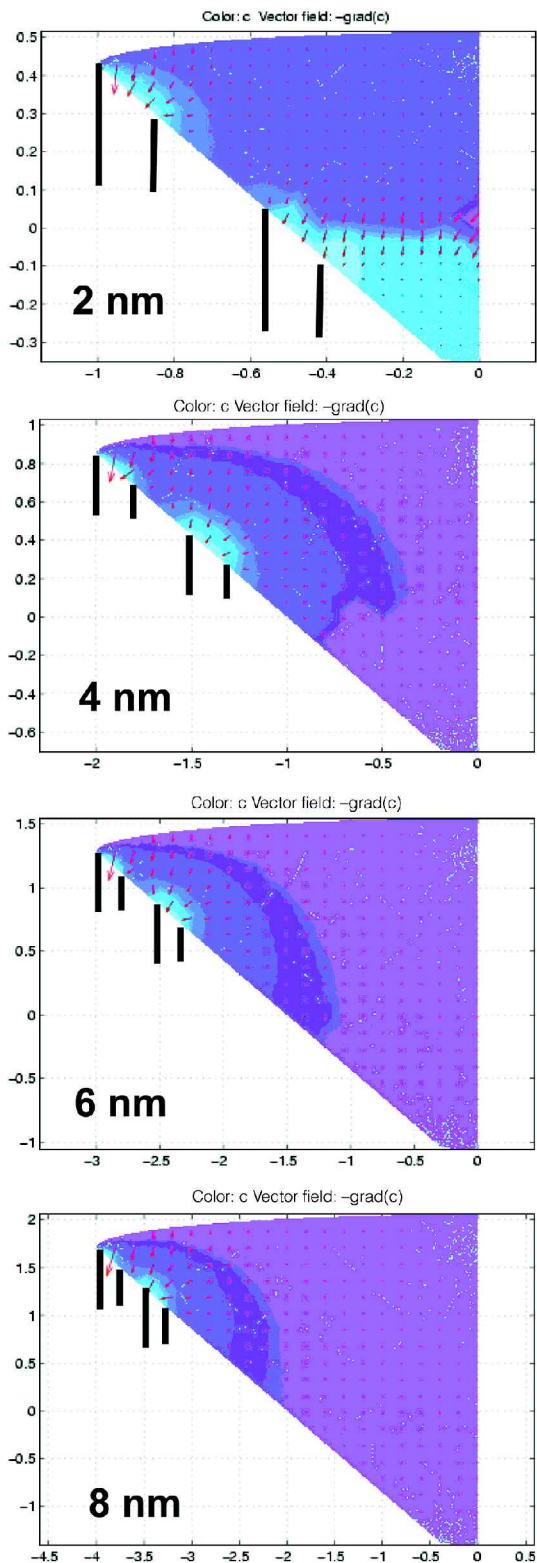
Nevertheless, there can be several reasons why the present simulations and experiments might not agree. For example, we have considered only diffusion, and the growth process itself might not be diffusion limited. In fact, the experiments of Hafner et al.<sup>14</sup> show that CNT growth is reaction-limited under certain conditions. Also, the diffusion coefficient is a function of both temperature and car-

bon concentration, and in the current study only the temperature dependence has been used because the effects of carbon concentration for the whole range are not available. Another reason might be that surface carbide formation ties up some of the carbon, effectively reducing the concentration at the front surface.

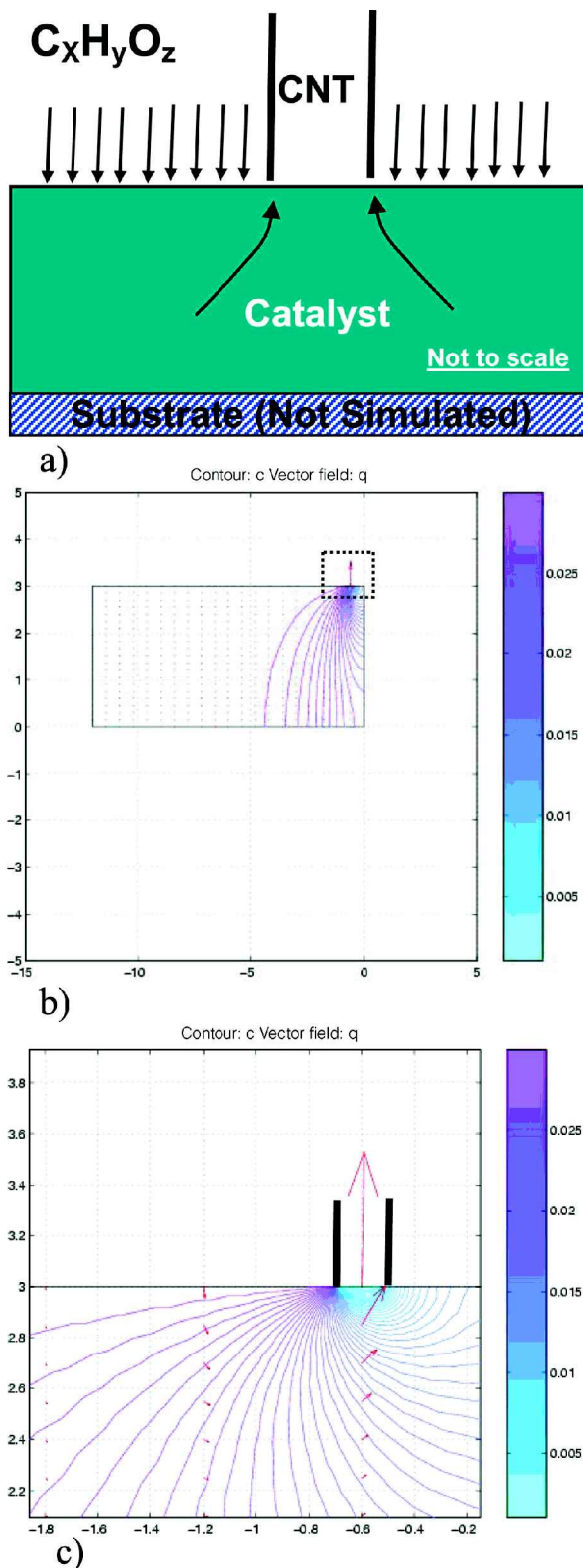
Of course, there are other reasons. However, the most intriguing possibility for the differences is that, in the absence of *in situ* measurements, the time-averaged growth rate calculated in the previous experiments might be different from the actual microscopic behavior. The kinetic Monte Carlo simulations of Grujicic et al.<sup>10</sup> indicate the nonlinear growth of NTs, and thus time-averaged growth measurements might not be useful in determining the growth phenomena and not conducive to direct comparisons with models. This is why the results of Geohegan et al.<sup>17</sup> are important. The issue of growth rates is fundamental for the simulations, and it is imperative that well-characterized and reliable direct measurements of it be available. Future simulations can ascertain how other physical processes control the growth in various situations once the rates are firmly established.

Figure 9 shows the calculated carbon concentration and concentration gradients for several double-walled nanotubes (DWNTs). The size of the catalyst particle is varied from 2 to 8 nm. DWNT simulations are performed in a manner similar to the approach for SWNTs but with the additional prescription of the location of the second wall based on the interatomic distance between NT walls. This location has Dirichlet BCs similar to the BCs of the first wall. For the smallest particle, the lower region of the catalyst particle is not saturated with carbon because the flux through the top surface is rapidly consumed to support formation of the DWNT. In this case even though the second wall is prescribed, there is not enough carbon flux to support a DWNT. However, as the catalyst particle size increases to 4, 6, and 8 nm, the lower part of the particle also becomes saturated and acts as a carbon reservoir for additional NT walls, so that the growth of the tubes is sustained. Thus, the current model, although it provides only for mass diffusion, gives insight into the conditions for formation of DWNTs and points to a possible reason why it is not common to see them with small catalytic particles.

Finally, with this model we explored what happens in a root-growth scenario. From a diffusion-limited perspective, the carbon diffuses into and through the nickel catalyst and then precipitates back onto the surface, as illustrated in the schematic diagram in Figure 10a. Here only the catalyst of thickness 3 nm is modeled, assuming that the substrate is a thermal bath corresponding to the catalyst temperature of 1000 K and that carbon does not diffuse into the substrate. Figure 10b shows the carbon concentration and gradients in the catalyst and how carbon diffuses to the prespecified location of CNT formation. Figure 10c, corresponding to the inset shown in Figure 10b, shows an enlarged plot around



**Fig. 9.** Carbon concentration (filled contours) and gradient distribution (arrows) in the catalyst particle for a DWNT with different outer diameters. Here the carbon concentration and gradient are plotted for four different particle diameters (2, 4, 6, and 8 nm). The 2-nm particle is depleted of carbon and that might indicate that DWNT formation for a 2-nm particle is least probable.



**Fig. 10.** Root-growth model for catalyst thickness of 3 nm and with  $T = 1000K$ : (a) schematic diagram; (b) simulation results with carbon concentration (filled contours) and gradient distribution (arrows) in the catalyst; (c) magnified view of the inset in (b). Here the carbon dissociates at the catalyst surface and diffuses through the bulk of the catalyst and precipitates at conductive locations on the surface.

the nanotube that is being extruded from the substrate. The reason for including this case in the current article is to illustrate the similarities between root and tip-growth mechanisms. In root growth, the carbon dissociates at the surface, diffuses through the bulk, and precipitates in CNTs at certain preferential locations. This is very similar to the tip-growth mechanism studied at length in this article. Further studies have to be performed to understand why carbon prefers to precipitate at certain locations on the surface. Appropriate continuum treatments can be developed to make this approach a more predictive tool, rather than a priori fixing the location and size of the growing nanotube.

## 5. SUMMARY AND FUTURE WORK

As part of a focused computational effort on the multi-scale simulations of carbon nanotube nucleation and growth, we have developed and applied computer programs for coupled heat and mass flow in one and two dimensions. Our preliminary results clearly illustrate the crucial role carbon diffusion plays in the growth of nanotubes, and they explain a number of the experimentally observed growth phenomena. Results to date also demonstrate the key roles played by the size and shape of the catalytic particle in conjunction with the concentration gradients at the gas–solid interface and in region 2. With the current set of assumptions, the CNT growth rate is linearly proportional to the surface carbon mass fraction, inversely proportional to the square of the diameter of the CNT–catalyst particle, and exponentially related to the catalyst temperature. Other results suggest how the growth of a single wall may interfere with, but not necessarily prevent, the growth of additional walls in a multi-walled nanotube. The size of the catalyst plays an important role in determining the number of walls in MWNTs because the catalyst acts like a reservoir for the carbon. In addition, we have found that the root-growth mechanism is quite similar to the tip-growth mechanism from a diffusion perspective. Again, the carbon concentration profile in the catalytic particle at the different growth sites is a key factor.

Although it is apparent that an impressive amount of insight can be obtained from simple continuum calculations of the type described above, the need for going beyond this simple approach is apparent. We want to incorporate more effectively the input from first-principles (e.g., density functional theory) electronic structure and MD calculations and to focus on the most reliable experimental data obtained under well-defined conditions.

We intend to implement a “rule-based approach” to incorporate this input, especially in studying the interfacial effects between regions. By this we mean that a set of rules will be established, specifying transitions that will occur in

any finite element cell based on the conditions in that cell and its immediate neighbors.

Inlet chemistry composition and decomposition in region 1 will be modeled and the possible formation of carbide layers considered in much more detail. After that, extensive parameter studies will be performed to identify the rate-limiting step under various conditions. We anticipate that knowledge gained from these studies will lead to the development of more rigorous multi-scale approaches.

**Acknowledgments:** This work was supported by the Laboratory Directed Research and Development (LDRD) program at Oak Ridge National Laboratory (ORNL), managed by UT-Battelle for the U.S. Department of Energy under Contract DE-AC05-00OR22725. Accordingly, the U.S. Government retains a non-exclusive, royalty-free license to publish or reproduce the published form of this contribution, or allow others to do so, for U.S. Government purposes.

We thank J. C. Wells, D. B. Geohegan, A. Puzos, and G. Eres for useful discussions on a number of issues.

## References and Notes

1. R. T. K. Baker, *Encyclopedia of Materials: Science and Technology*, Elsevier Science Ltd., Amsterdam (2001), pp. 932–941.
2. S. Subramoney, *Encyclopedia of Materials: Science and Technology*, Elsevier Science Ltd., Amsterdam (2001), pp. 941–952.
3. D. B. Hash and Meyyappan, *J. Appl. Phys.* **93**, 750 (2003).
4. A. M. Cassell, J. A. Raymakers, J. Kong, and H. Dai, *J. Phys. Chem. B* **103**, 6484 (1999).
5. Y. Li, W. Kim, Y. Zhang, M. Rolandi, D. Wang, and H. Dai, *J. Phys. Chem. B* **105**, 11424 (2001).
6. R. T. K. Baker and P. A. Harris, *Chemistry and Physics of Carbon*, edited by P. L. Walker and P. A. Throer, Marcel Dekker, New York (1978), Vol. 14, pp. 83–165.
7. K. P. D. Jong, and J. W. Geus, *Catal. Rev.-Sci. Eng.* **42**, 481 (2000).
8. J.-C. Charlier and S. Iijima, *Carbon Nanotubes*, Topics in Applied Physics, edited by M. S. Dresselhaus, G. Dresselhaus, and Ph. Avouris, Springer-Verlag, Berlin (2001), Vol. 80, pp. 55–81.
9. H. Dai, *Carbon Nanotubes*, Topics in Applied Physics, edited by M. S. Dresselhaus, G. Dresselhaus, and Ph. Avouris, Springer-Verlag, Berlin (2001), Vol. 80, pp. 29–53.
10. M. Grujicic, G. Cao, and B. Gersten, *Mater. Sci. Eng. B* **94**, 247 (2002).
11. I. Alstrup, *J. Catal.* **109**, 241 (1988).
12. P. Chitrapu, C. R. F. Lund, and J. A. Tsamopoulos, *Carbon* **30**, 285 (1992).
13. S. A. Safvi, E. C. Bianchini, and C. R. F. Lund, *Carbon* **29**, 1245 (1991).
14. J. H. Hafner, M. J. Bronikowski, B. R. Azamian, P. Nikolaev, A. G. Rinzler, D. T. Colbert, K. A. Smith, and R. E. Smalley, *Chem. Phys. Lett.* **296**, 195 (1998).
15. *CRC Materials Science and Engineering Handbook*, CRC Press, Boca Raton, FL (1994).
16. M. Chhowalla, K. B. K. Teo, C. Ducati, N. L. Rupesinghe, G. A. J. Amaratunga, A. C. Ferrari, D. Roy, J. Robertson, and W. I. Milne, *J. Appl. Phys.* **90**, 5308 (2001).
17. D. B. Geohegan, A. A. Puzos, I. N. Ivanov, S. Jesse, G. Eres, and J. W. Howe, Submitted for publication.